

Exploring intermediate temperature reactivity: Experimental and kinetic modeling insights into 50/50% blend of methyl butanoate and methyl crotonate

Lalit Y. Attarde^{a,*}, Praise Noah Johnson^b, Sonal Kumar Vallabhuni ^c, R.X. Fernandes ^c,
Krithika Narayanaswamy ^a

^a*Department of Mechanical Engineering, Indian Institute of Technology Madras, Chennai, India*

^b*Department of Mechanical Engineering, University of Minnesota, Minneapolis, United States*

^c*Physikalisch-Technische Bundesanstalt, Department of Physical Chemistry, Braunschweig, Germany*

Contents

1. Model validation with respect to experimental studies for methyl butanoate
 - (a) High temperature ignition delay time
 - (b) Laminar flame speeds
 - (c) Burner stabilised flames
 - (d) Counter-flow diffusion flames
 - (e) Intermediate temperature ignition delay times
 - (f) Variable pressure flow reactor
 - (g) Jet stirred reactor
 2. Model validation with respect to experimental studies for methyl crotonate
 - (a) High temperature ignition delay time
 - (b) Laminar flame speeds
 - (c) Burner stabilised flames
 - (d) Counter-flow diffusion flames
 - (e) Intermediate temperature ignition delay times
 - (f) Jet stirred reactor
 3. Sensitivity analysis for blend of methyl butanoate and methyl crotonate
 4. Effect of composition of mixture of MB and MB2D on reactivity at high temperatures
 5. Comparison of performance of current kinetic model and literature models
 - (a) Quantitative analysis of model's performance
 - (b) Comparison of predictions by literature models against RCM experimental studies
 6. Path flux analysis
 7. Effect of cross reactions on prediction of experimental data for blend of MB and MB2D
 8. List of newly added reactions
-

1. Model validation with respect to experimental studies for methyl butanoate

1.1. High temperature ignition delay times

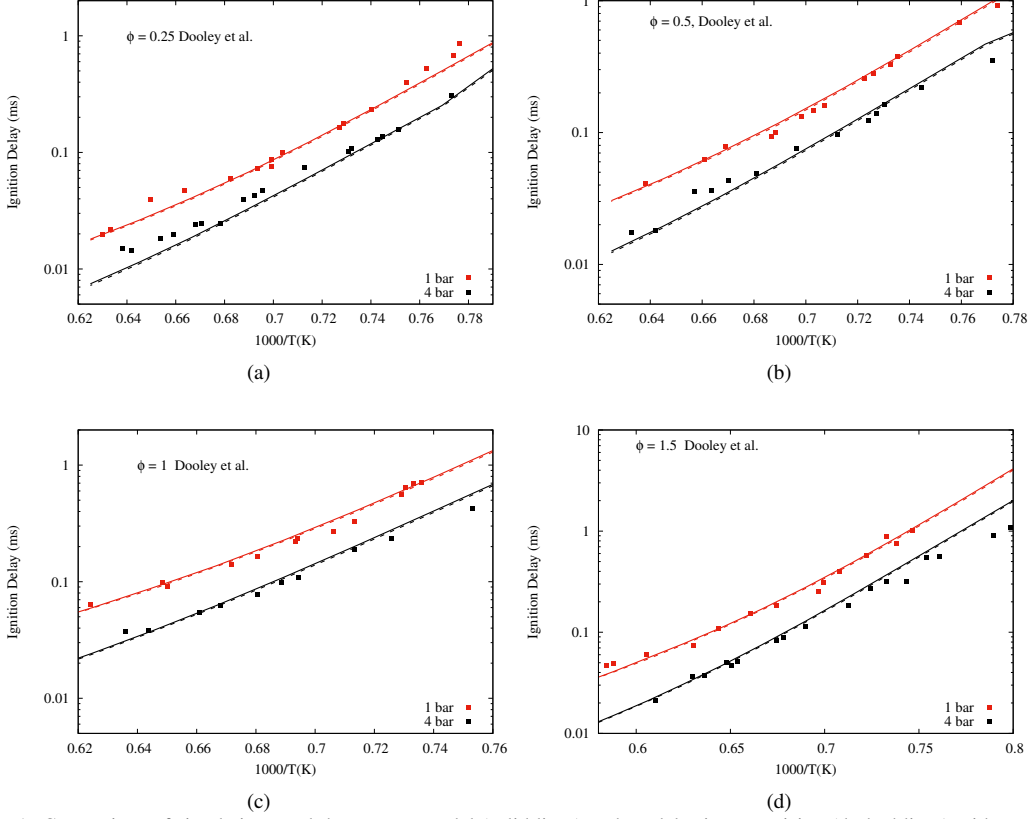


Fig. 1: Comparison of simulation result by present model (solid lines) and model prior to revision (dashed lines) with respect to shock tube ignition delay (symbols) measured by dooley et al. [1]. Simulation and experiments are performed for oxidation of mixture of MB/O₂/Ar at 1 bar and 4 bar for different equivalence ratios of (a) $\phi = 0.25$, (b) $\phi = 0.5$, (c) $\phi = 1.0$, and (d) $\phi = 1.5$. Ignition delay are calculated at the time required to reach the instant of maximum rate of rise in the CH radicals.

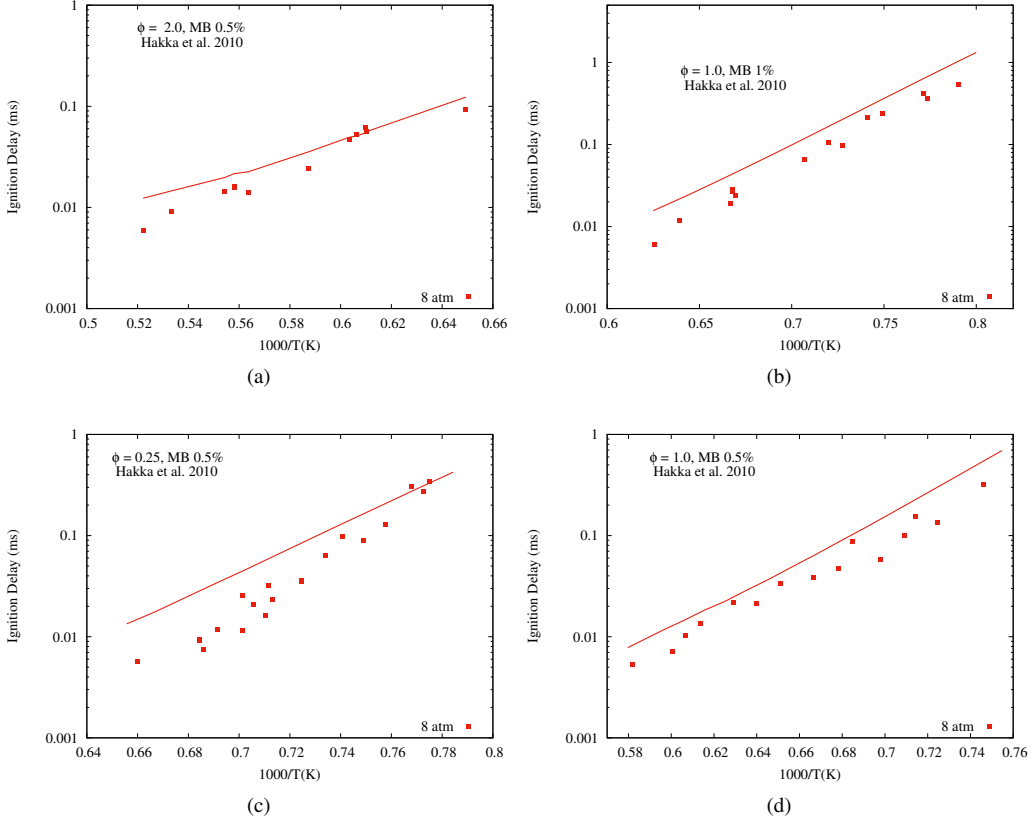


Fig. 2: Comparison of experimental ignition delays (symbols) measured in shock tube [2] and simulation results (lines) produced for oxidation of MB at different equivalence ratios and fuel mole fractions of (a) $\phi = 2$, MB 0.5%, (a) $\phi = 1$, MB 1%, (a) $\phi = 0.25$, MB 0.5%, and (a) $\phi = 1.0$, MB 0.5%.

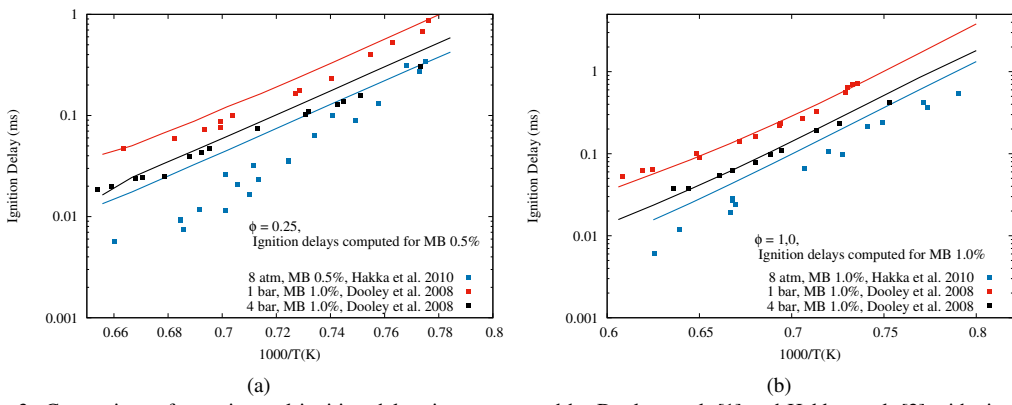


Fig. 3: Comparison of experimental ignition delay times measured by Dooley et al. [1] and Hakka et al. [2] with simulated ignition delays using present model.

1.2. Laminar flame speeds

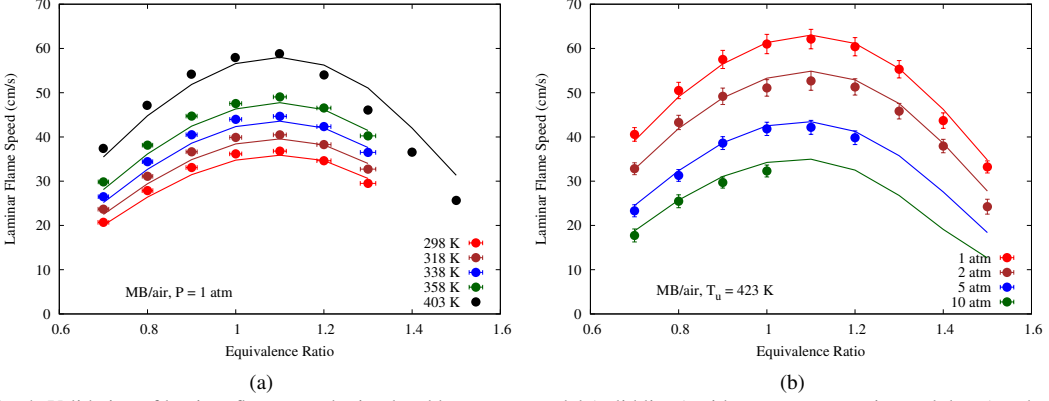


Fig. 4: Validation of laminar flame speeds simulated by current model (solid lines) with respect to experimental data (symbols) for range of pressures (1-10 atm) and unburnt temperatures (T_u) (298-423 K). Plot (a) includes validation of experiments by Konnov et al. [3] for $T_u = 298\text{-}358 \text{ K}$ and Wang et al. [4] for $T_u = 403 \text{ K}$. Plot (b) includes validation of experiments by Li et al. [5] for pressures spanning from 1 atm to 10 atm.

1.3. Burner stabilised flames

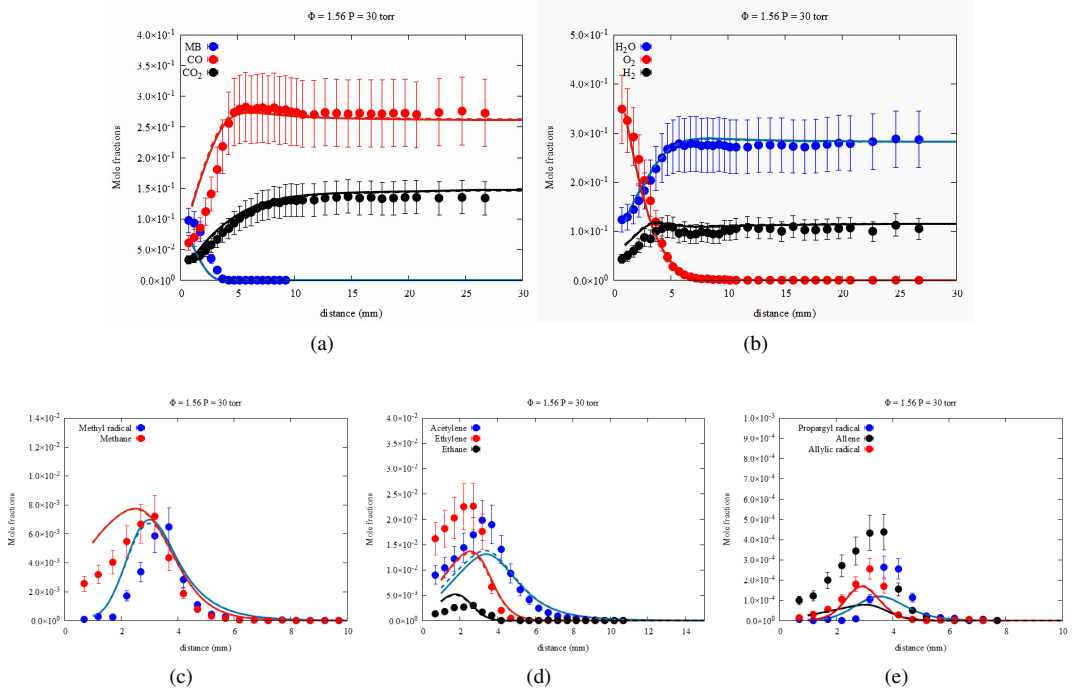


Fig. 5: Species mole fraction (X_i) predictions by present model (solid lines) and pre-revised model (dashed lines) compared to experimental data points measured in the burner stabilised configuration by Yang et al. [6] for MB/O₂/Ar mixture.

1.4. Counter-flow diffusion flames

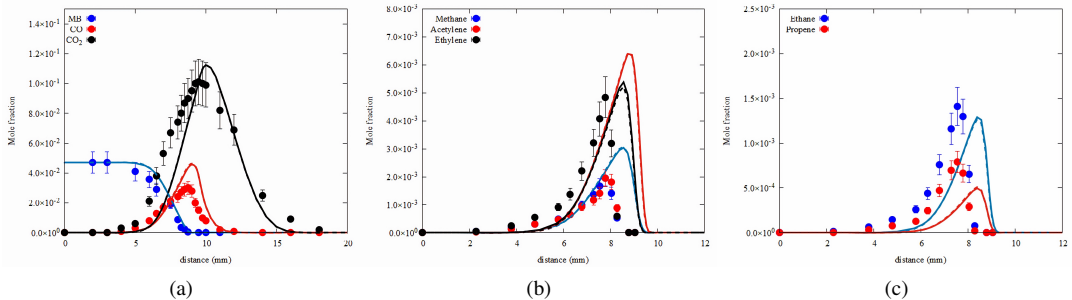


Fig. 6: Species mole fraction predictions by present model (solid lines) and pre-revised model (dashed lines) compared to experimental data points measured in the counter-flow flames configuration by Sarathy et al. [6] for oxidation of MB.

1.5. Intermediate temperature ignition delay times

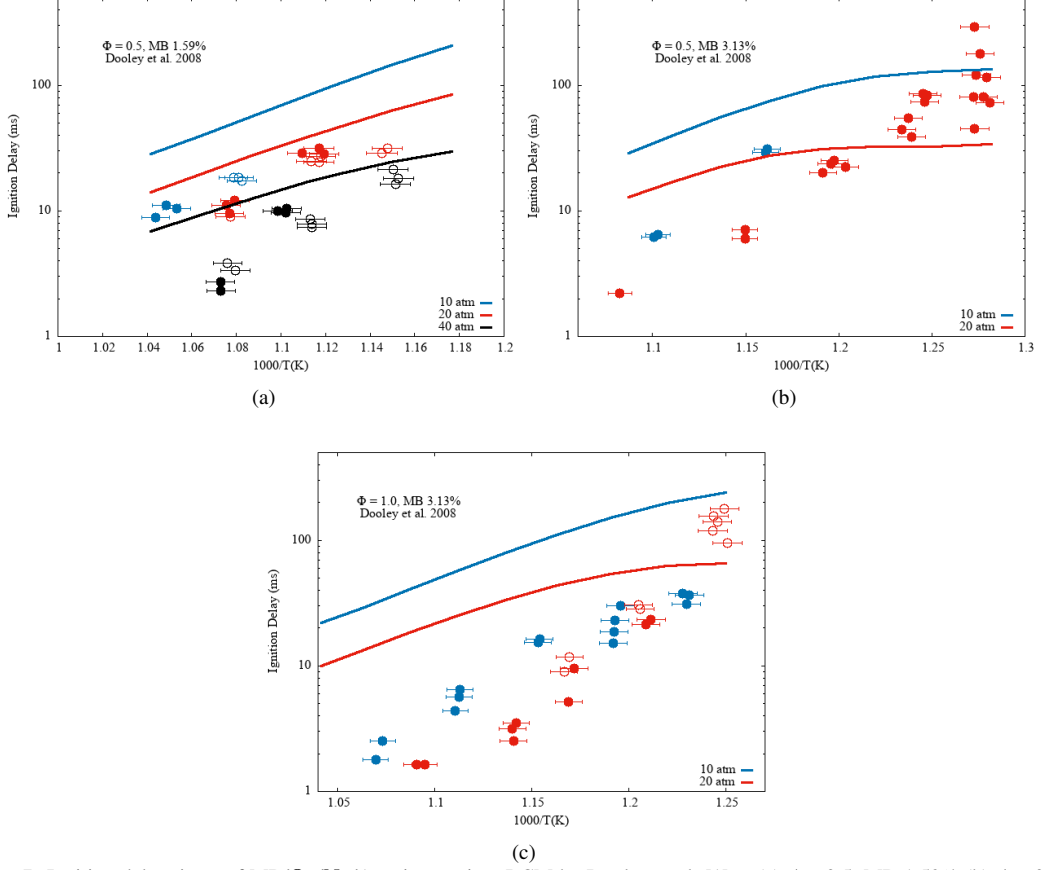


Fig. 7: Ignition delay times of MB/O₂/N₂/Ar mixtures in a RCM by Dooley et al. [1] at (a) $\phi = 0.5$, MB 1.59% (b) $\phi = 0.5$, MB 3.13% and (c) $\phi = 1.0$, MB 3.13% for different pressures. Solid and hollow symbols corresponds to experimental ignition delays measured using diluent Argon alone and mixture of Nitrogen and Argon respectively.

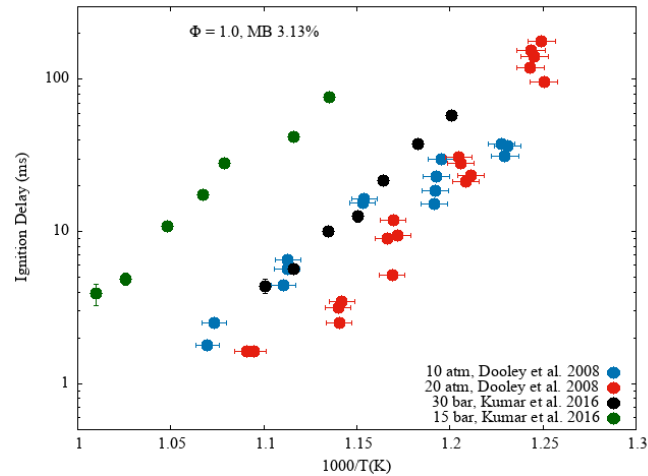


Fig. 8: Comparison of experimental ignition delay times of MB/O₂/Ar mixtures in a RCM measured by Dooley et al. [1] and Kumar et al. [7] at 3.13% of MB and stoichiometric condition.

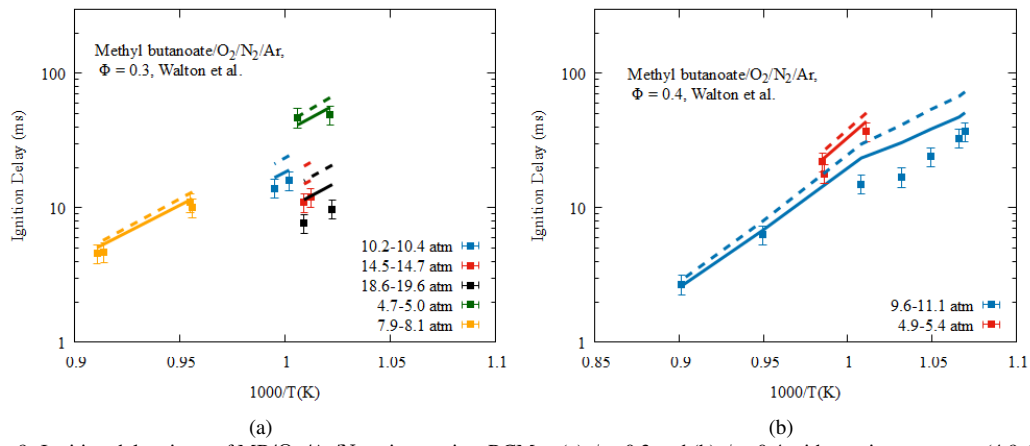


Fig. 9: Ignition delay times of MB/O₂/Ar/N₂ mixtures in a RCM at (a) $\phi = 0.3$ and (b) $\phi = 0.4$ with varying pressures (4.9-19.6 atm). Symbols corresponds to experiment from Walton et al. [8] and adiabatic simulation results using the present model (solid lines) and model prior to revision (dashed lines).

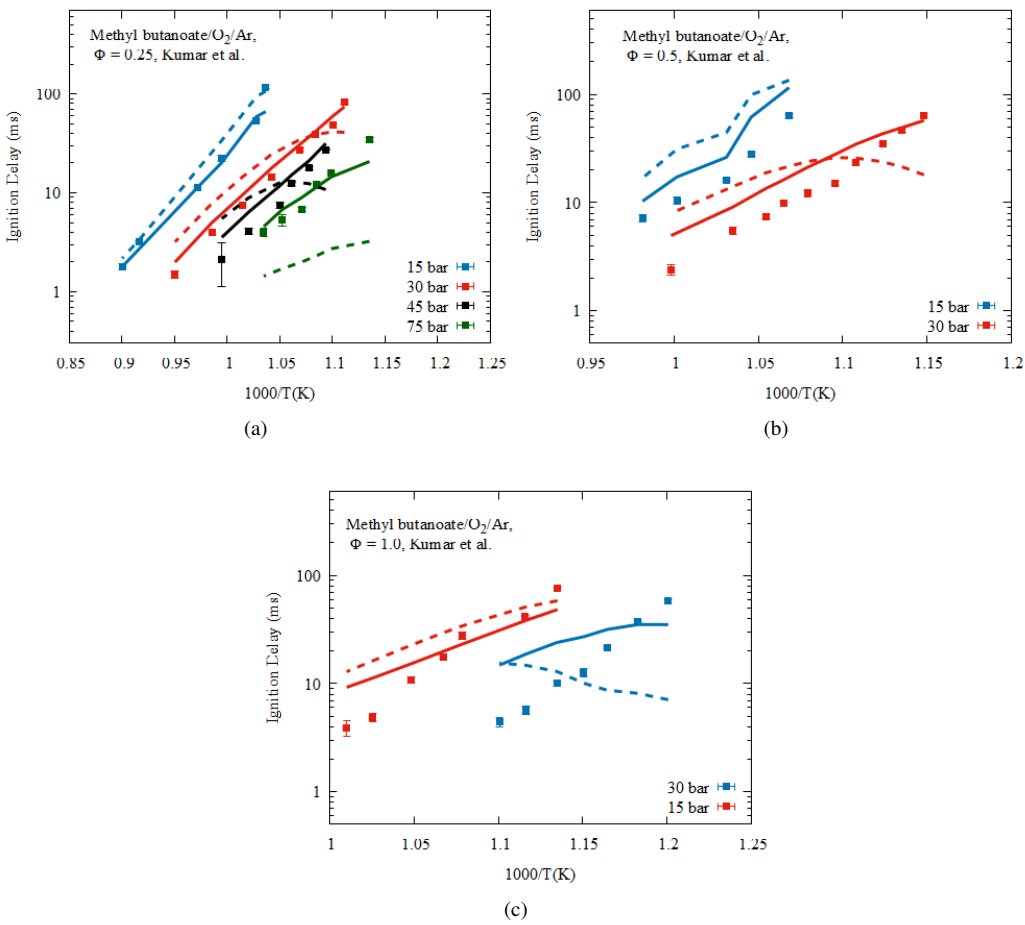


Fig. 10: Ignition delay times of MB/O₂/Ar mixtures in a RCM at (a) $\phi = 0.25$, (b) $\phi = 0.5$, (c) $\phi = 1.0$ with varying pressures (15-75 bar). Symbols corresponds to experiment from Kumar et al. [7] and simulation results using the present model (solid lines) and model prior to revision (dashed lines).

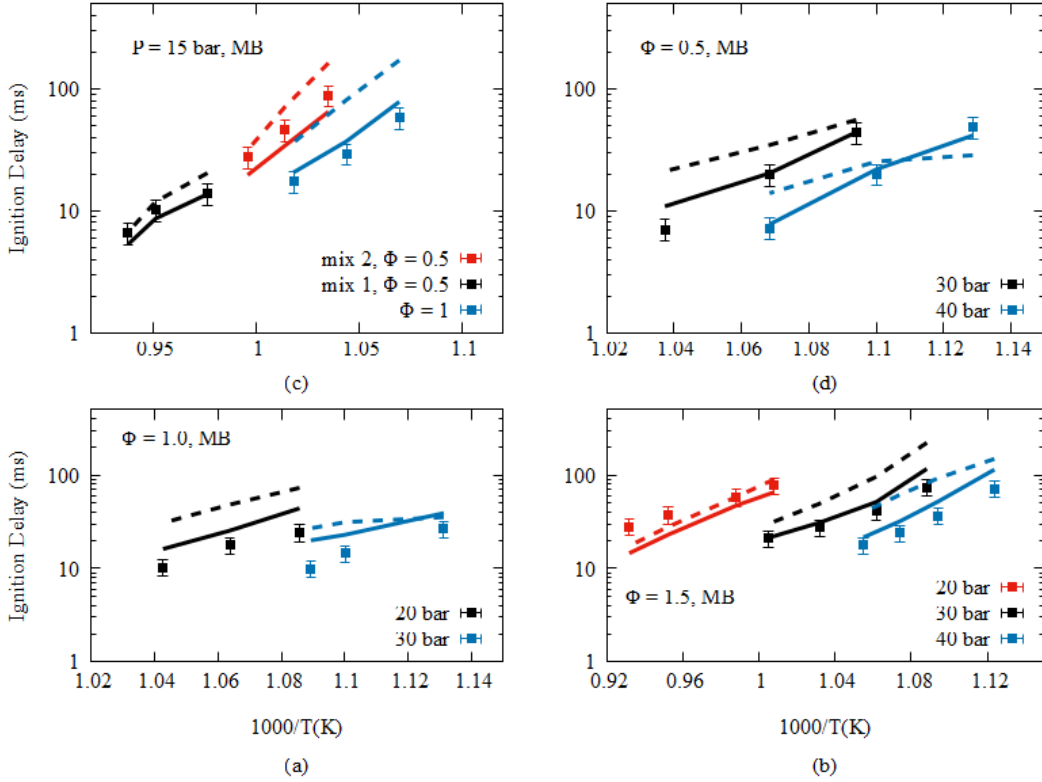


Fig. 11: Ignition delay times of MB/O₂/Ar/N₂ mixtures in a RCM at (a) $\phi = 1.0$, (b) $\phi = 1.5$, (c-d) $\phi = 0.5$ with varying pressures (15-40 bar). Symbols corresponds to experiment (uncertainty of 20%) from Lele et al. [9] and simulation results using the present model (solid lines) and pre-revised model (dashed lines).

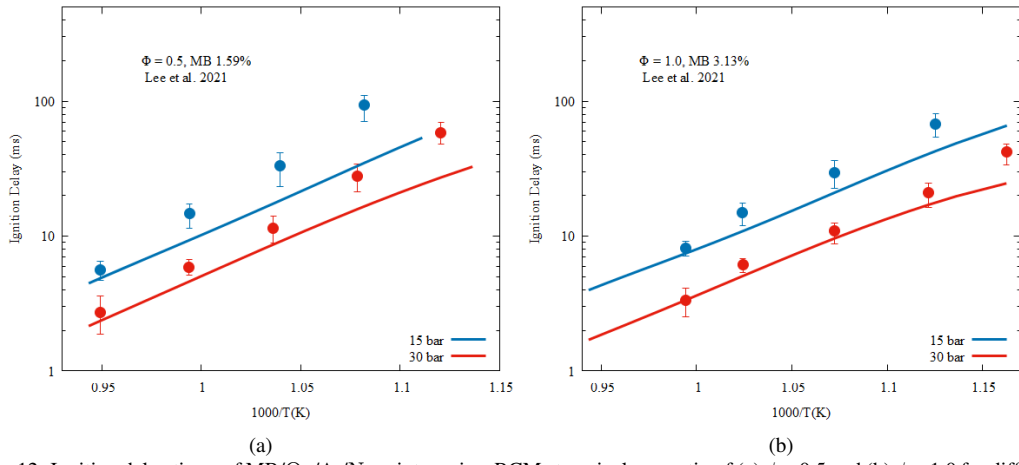


Fig. 12: Ignition delay times of MB/O₂/Ar/N₂ mixtures in a RCM at equivalence ratio of (a) $\phi = 0.5$ and (b) $\phi = 1.0$ for different pressures of 15 and 30 bar. Symbols corresponds to experiment from Lee et al. [10] and ignition delays are computed for 50/50% composition of Argon and Nitrogen using the present model (solid lines) with an isochor homogeneous adiabatic reactor.

1.6. Variable pressure flow reactor

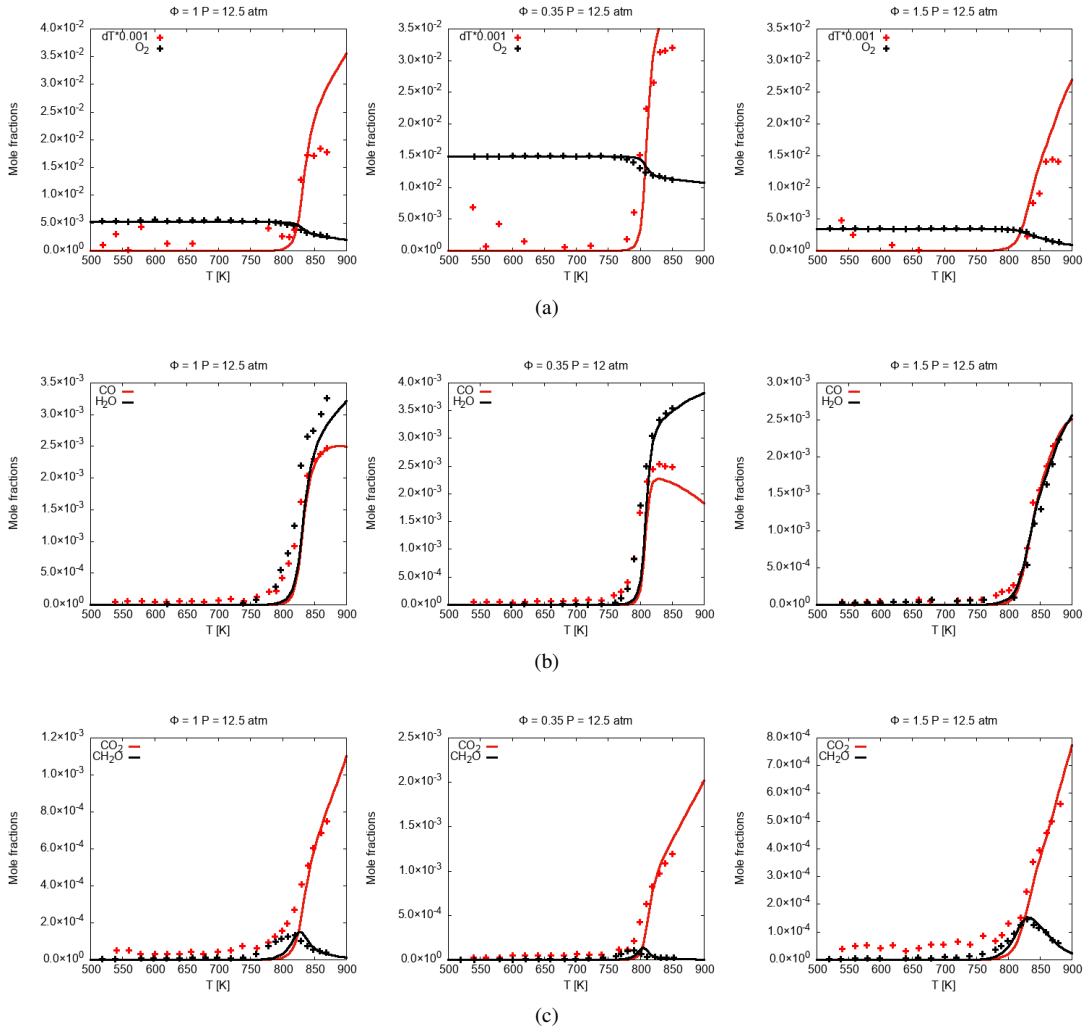


Fig. 13: Mole fraction profiles of major intermediates produced in MB oxidation in variable pressure flow reactor at varying equivalence ratios (0.35, 1.0, 1.5), and pressure = 12.5 atm. Model simulations: solid lines, experimental data [11]: symbols

1.7. Jet stirred reactor

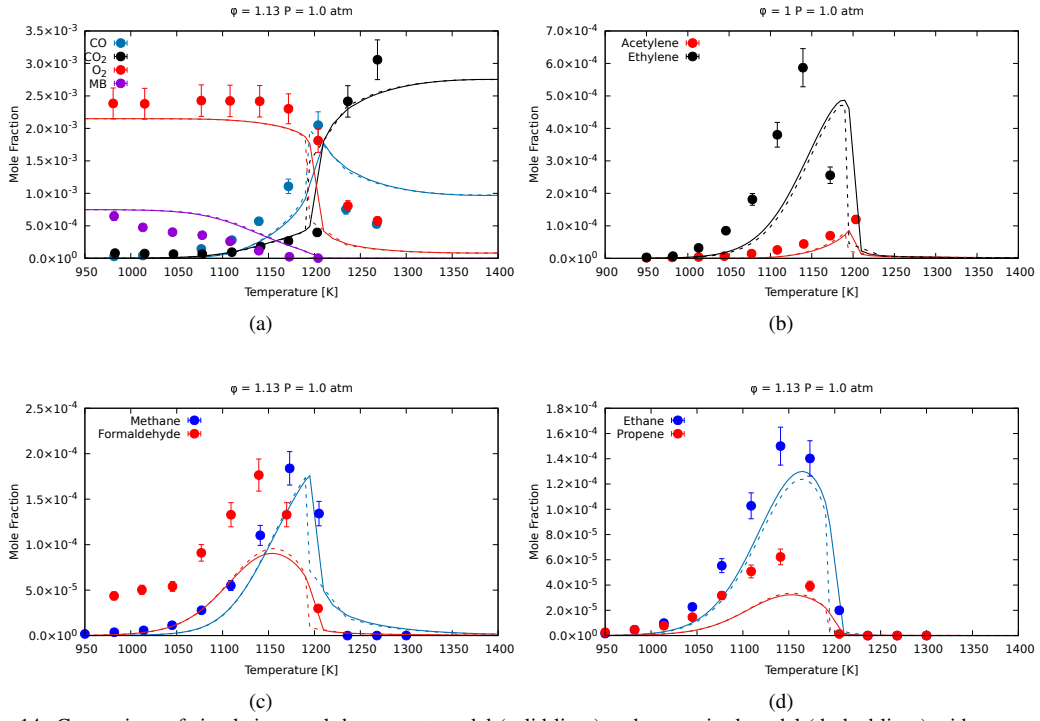


Fig. 14: Comparison of simulation result by present model (solid lines) and pre-revised model (dashed lines) with respect to mole fractions of species (symbols) measured by Gail et al. [12] in the jet stirred reactor for residence time of 0.07 seconds.

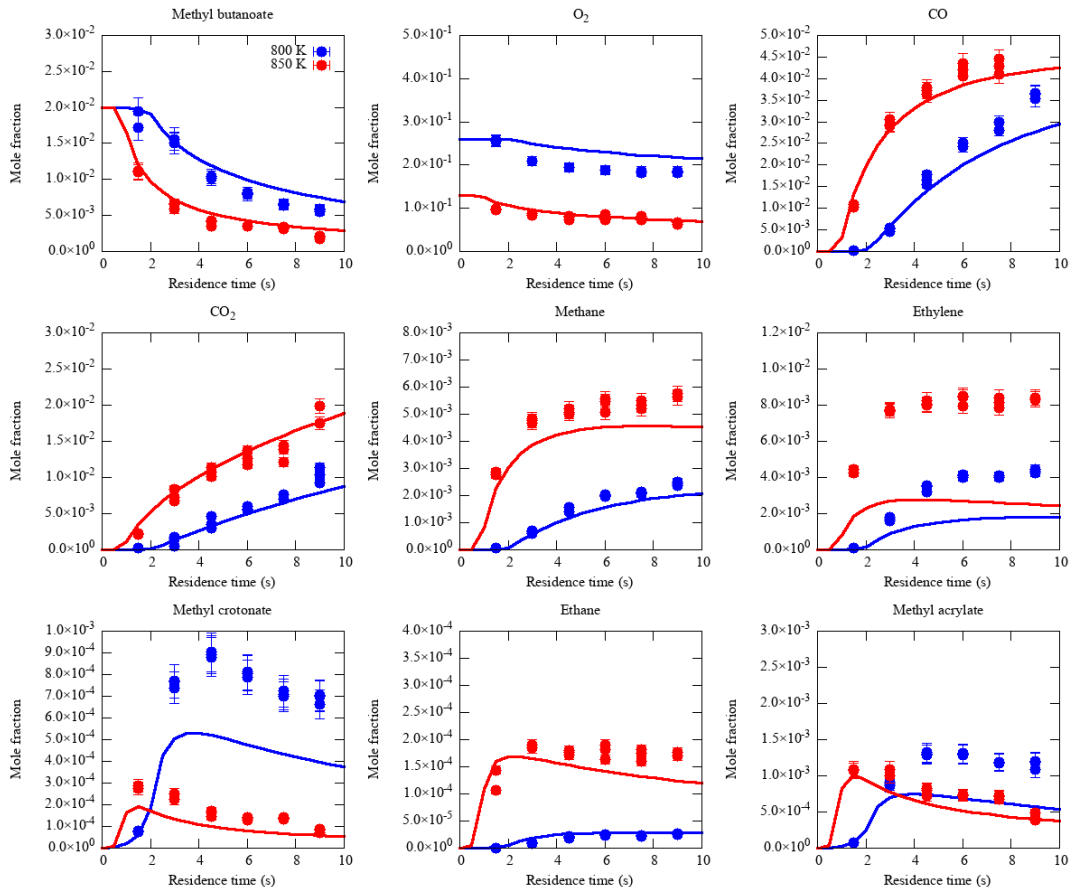


Fig. 15: Comparison of simulation result by present model (solid lines) and experimental mole fractions of species (symbols) measured by Hakka et al. [2] in the jet stirred reactor for varying residence times at 800K, $\phi = 0.5$ (blue) and 850 K, $\phi = 1.0$ (red)

2. Model validation with respect to experimental studies for methyl crotonate

2.1. High temperature ignition delay times

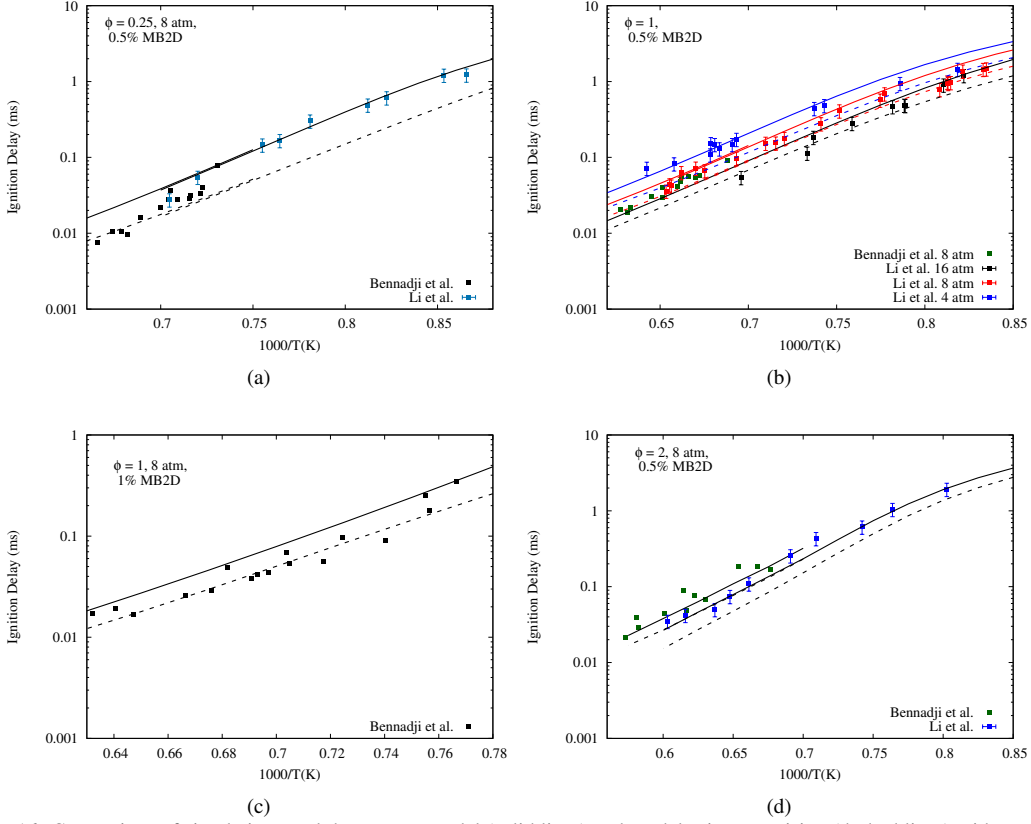


Fig. 16: Comparison of simulation result by present model (solid lines) and model prior to revision (dashed lines) with respect to shock tube ignition delay (symbols) measured by bennadji et al. [13] and Li et al. [14]. Simulation and experiments are performed for oxidation of mixture of MB2D/O₂/Ar for different equivalence ratios of (a) $\phi = 0.25$, (b-c) $\phi = 1.0$, and (d) $\phi = 2.0$. Ignition delay are defined by the time required to reach 50% of the maximum OH concentration for experiments by Bennadji et al. [13] and time required to reach at onset of sudden rise in OH concentrations for experiments by Li et al.[14].

2.2. Laminar flame speeds

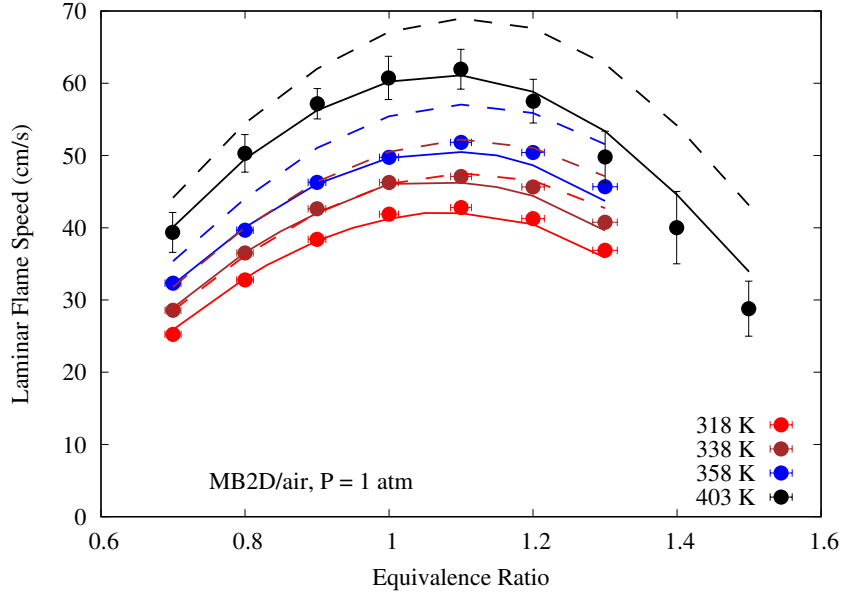


Fig. 17: Validation of laminar flame speeds simulated by current model (solid lines) with respect to experimental data (symbols) for pressure of 1 atm and range of unburnt temperatures (T_u) (318–403 K). Plot includes validation of experiments by Johnson et al. [15] for T_u = 318–358 K and Wang et al. [4] for T_u = 403 K.

2.3. Burner stabilised flames

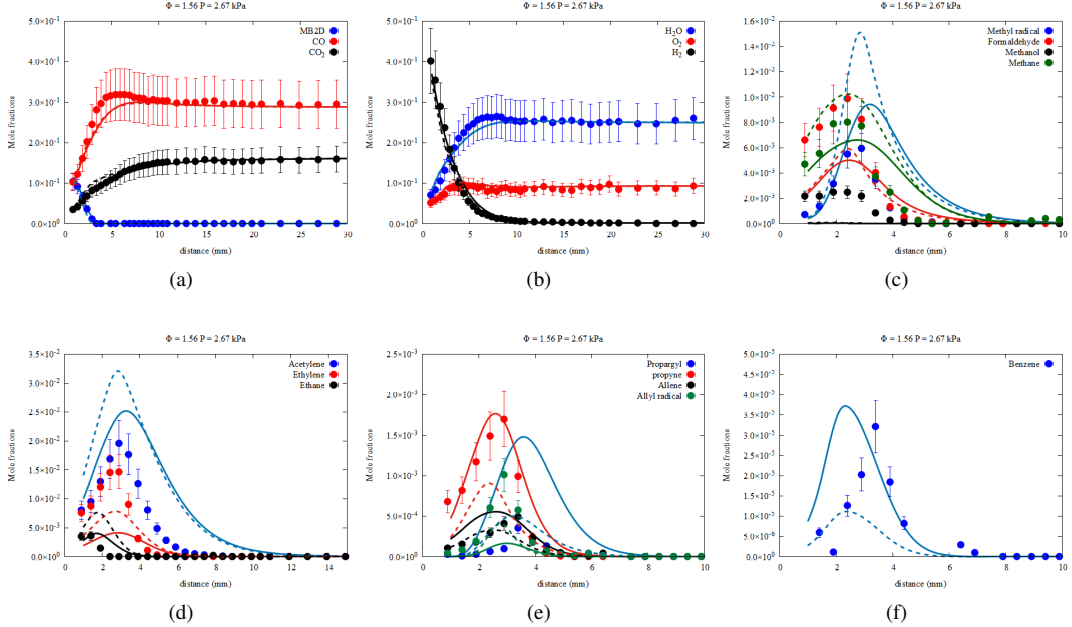


Fig. 18: Species mole fraction predictions by present model (solid lines) and pre-revised model (dashed lines) compared to experimental data points measured in the burner stabilised configuration by Yang et al. [16] for MB2D/O₂/Ar mixture.

2.4. Counter-flow diffusion flames

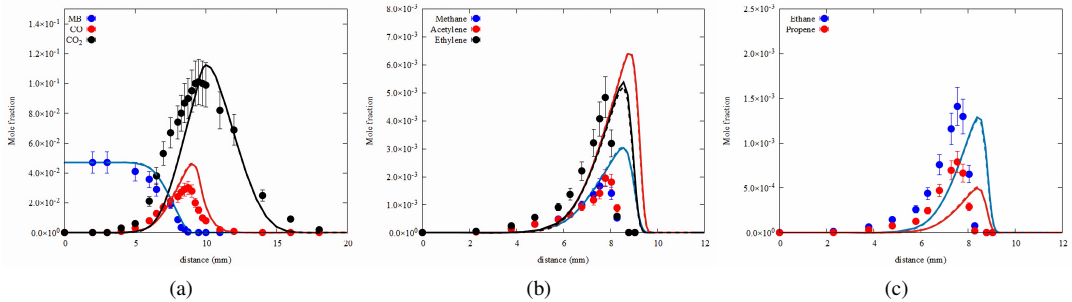


Fig. 19: Species mole fraction predictions by present model (solid lines) and pre-revised model (dashed lines) compared to experimental data points measured in the counter-flow flames configuration by Sarathy et al. [6] for oxidation of MB2D.

2.5. Intermediate temperature ignition delay times

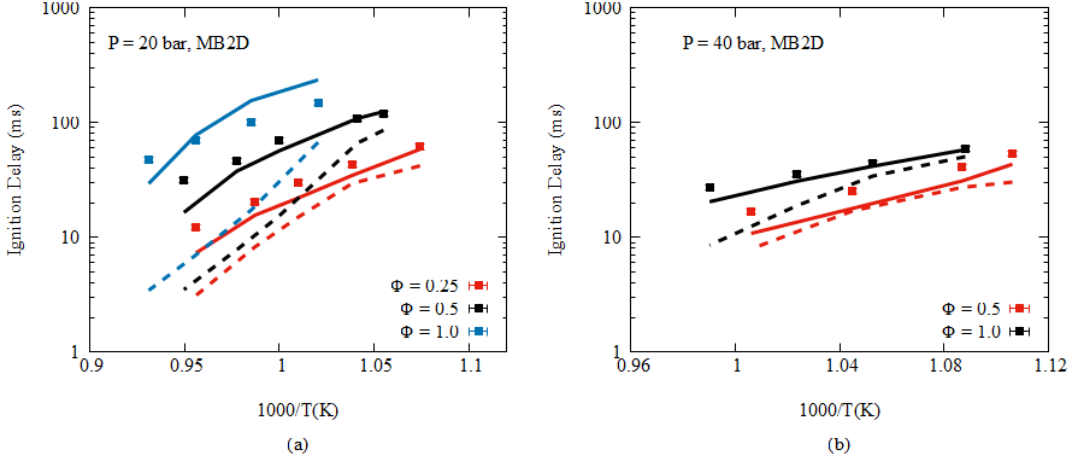


Fig. 20: Ignition delay times of MB2D/O₂/Ar/N₂ mixtures in a RCM at pressures of (a) $P = 20$ bar and (b) $P = 40$ bar for different equivalence ratios (0.25, 0.5, and 1.0). Symbols corresponds to experiment from Vallabhuni et al. [17] and simulation results using the present model (solid lines) and pre-revised model (dashed lines).

2.6. Jet stirred reactor

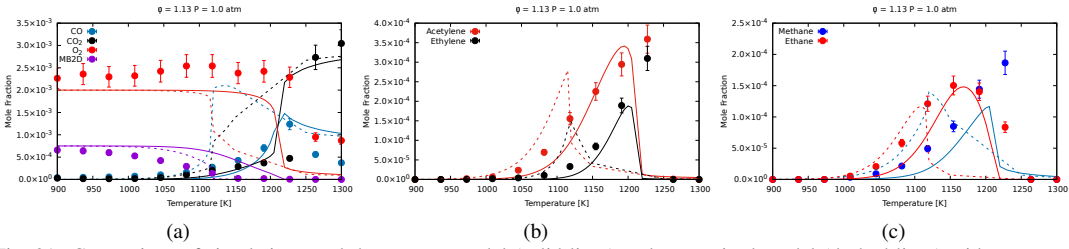


Fig. 21: Comparison of simulation result by present model (solid lines) and pre-revised model (dashed lines) with respect to mole fractions of species (symbols) measured by Gail et al. [12] in the jet stirred reactor for residence time of 0.07 seconds.

3. Sensitivity analysis for blend of methyl butanoate and methyl crotonate

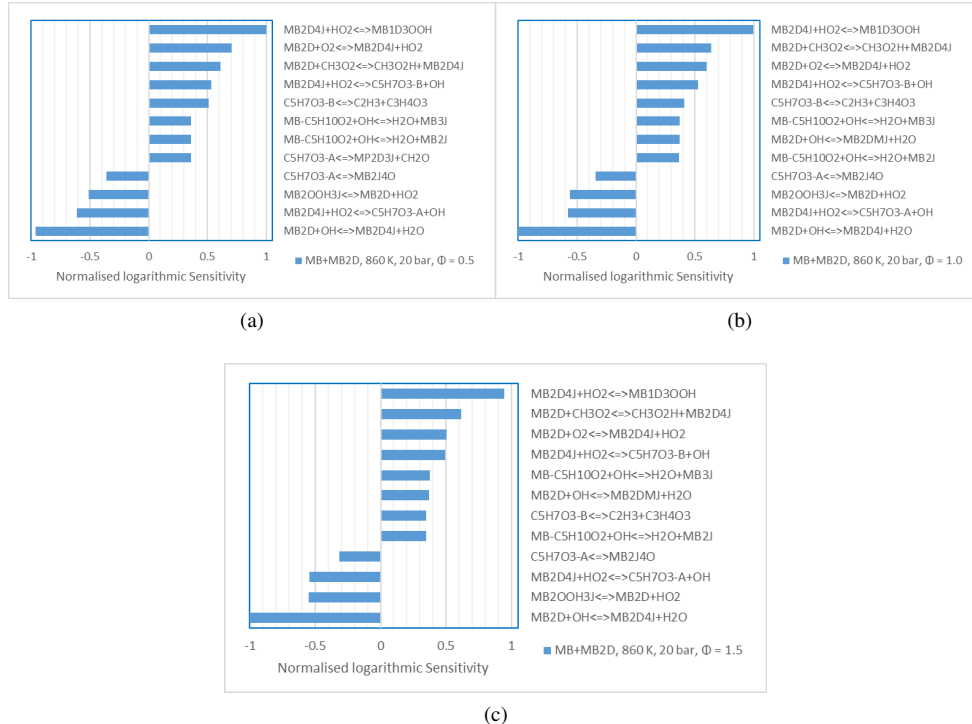


Fig. 22: Sensitivity analysis for hydroxyl radicals produced during oxidation of MB/MB2D mixture in N_2/Ar as diluents, calculated at the onset of sudden rise in hydroxyl radicals concentration using present model, at equivalence ratios of (a) $\phi = 0.5$, (a) $\phi = 1.0$, and (a) $\phi = 1.5$

4. Effect of varying composition of blend of MB and MB2D on reactivity at high temperatures

To thoroughly understand the reactivity trend of blend of MB and MB2D, we produced contour plots of around 1000 ignition delays for various mixture compositions of MB and MB2D across a temperature range of 1000 to 1600 K, as seen from the iso-lines in Fig. 23. Differently, above 1150 K, MB2D exhibits higher reactivity compared to MB. This new trend follows a monotonic increase in reactivity upon the addition of MB2D to the mixture. The presence of double bonds in MB2D leads to its higher reactivity at high temperatures as compared to MB [18]. This is because double bonds facilitate radical addition reactions, leading to the formation of various small active radicals. Moreover, the weak β C–H bond in MB2D and the resonantly stable allyl radicals make them prone to scission reactions, thereby producing an active pool of H atoms. Therefore, the addition of MB2D into the mixture results in an overall increase in reactivity of mixture at high temperatures.

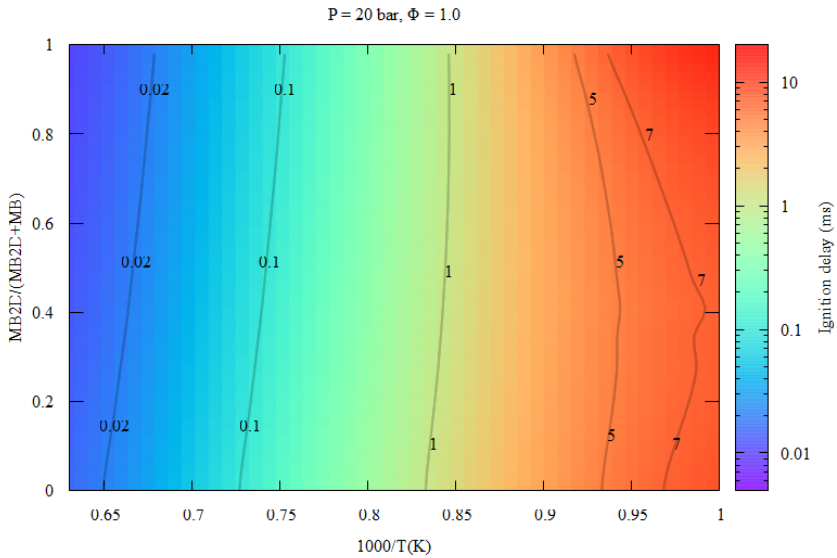


Fig. 23: Contour map of ignition delay times for different mixture of MB and MB2D at constant pressure (20 bar) and equivalence ratio ($\phi = 1.0$), for temperature range of 1000–1600 K.

5. Comparison of performance of current kinetic model and literature models

5.1. Quantitative analysis of model's performance

To quantify the performance of kinetic model more accurately, we have evaluated the error values produced by our present model and compared them with those from literature models [1, 9, 12, 15] for various RCM datasets. We employed the methodology proposed by Olm et al. [19] to calculate error function values between the model's predictions and experimental data using the following formula:

$$E_i = \frac{1}{N_i} \sum_{j=1}^{N_i} \left(\frac{Y_{ij}^{sim} - Y_{ij}^{exp}}{\sigma(Y_{ij}^{exp})} \right)^2$$

$$E = \frac{1}{N} \sum_{i=1}^N E_i$$

Where

$$Y_{ij} = \begin{cases} y_{ij} & \text{if } \sigma(y_{ij}^{exp}) \approx \text{constant} \\ \ln(y_{ij}) & \text{if } \sigma(\ln(y_{ij}^{exp})) \approx \text{constant} \end{cases}$$

N = Total number of datasets

N_i = Number of data points within the i th dataset

y_{ij} = j th data point in the i th dataset

$\sigma(Y_{ij}^{exp})$ = Standard deviation of experimental value

Here, Y_{ij} represents the logarithmic value of y_{ij} to achieve nearly constant standard deviation. We have conservatively considered an uncertainty of $\pm 20\%$ for experimental data by Kumar et al. [7] and Vallabhuni et al. [17], as they report uncertainty in T_c of $\pm 0.7\%$ [20] and 10 K respectively. Figure 24 displays error function values (E_i) for each RCM experiment datasets and overall error function values (E) for both current and literature kinetic models. The Johnson model [15] was compared against only MB2D experiments, as it was developed with a focus on improvement in kinetic of MB2D. Also, Dooley [1] and Lele model [9] were validated against MB experiments since respective studies centered around kinetics of MB. Present model produces overall lowest error values with average error of 2σ in predicting various experimental data and error values for predicting individual experimental dataset are shown in Table 1. It is to be noted that no volume profiles were available for RCM 427 experiments by Walton et al. [8] and Lee et al. [10]. Simulation results of different kinetic models and error function calculations are provided in the spreadsheet file of supplementary material.

Experimental dataset	Average error	Maximum error
Lele et al. [9]	1.7σ	3.3σ
Kumar et al. [7]	2.4σ	6σ
Walton et al. [8]	1.9σ	3.7σ
Lee et al. [10]	2.2σ	4.6σ
Johnson et al. [15]	1.6σ	2.5σ
Present experiments	1.8σ	3.3σ

Table 1: Error estimate between different experimental datasets and predictions of present kinetic model.

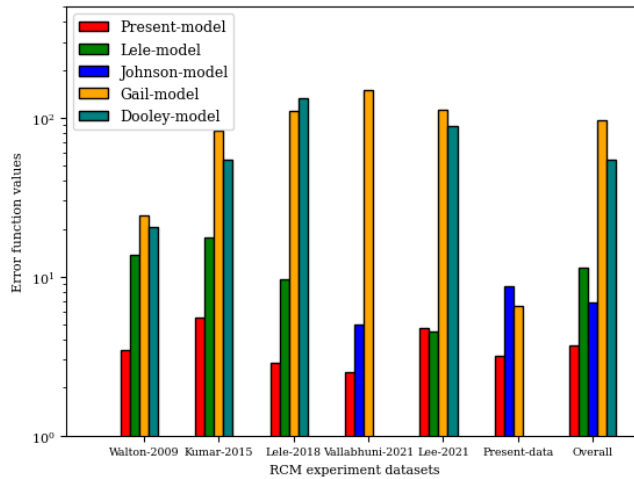


Fig. 24: Comparison of performance of different kinetic models produced in the literature, in predicting ignition delays measured in the RCM.

5.2. Comparison of predictions by literature models against RCM experimental studies

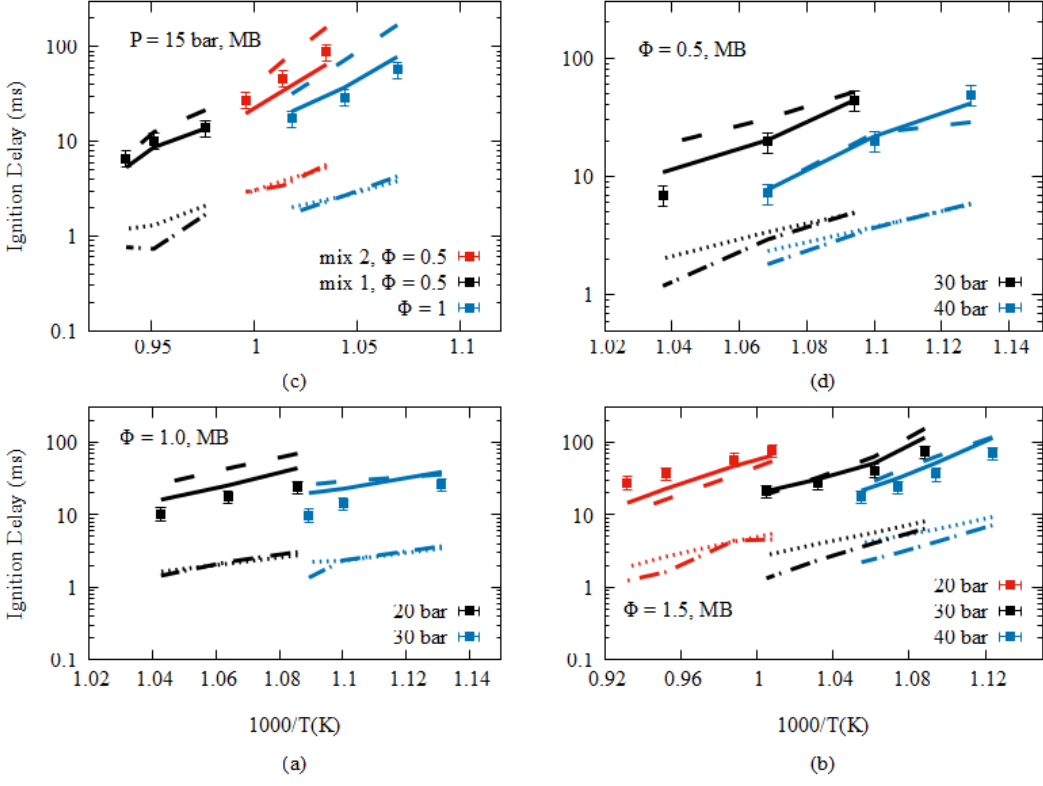


Fig. 25: Ignition delay times of MB/O₂/Ar/N₂ mixtures in a RCM at (a) $\phi = 1.0$, (b) $\phi = 1.5$, (c-d) $\phi = 0.5$ with varying pressures (15-40 bar). Symbols correspond to experiment from Lele et al. [9] and lines show simulation results using the present model (solid lines), Lele model (- - lines) [9], Gail model (.... lines) [12], and Dooley model (.-.-. lines) [1].

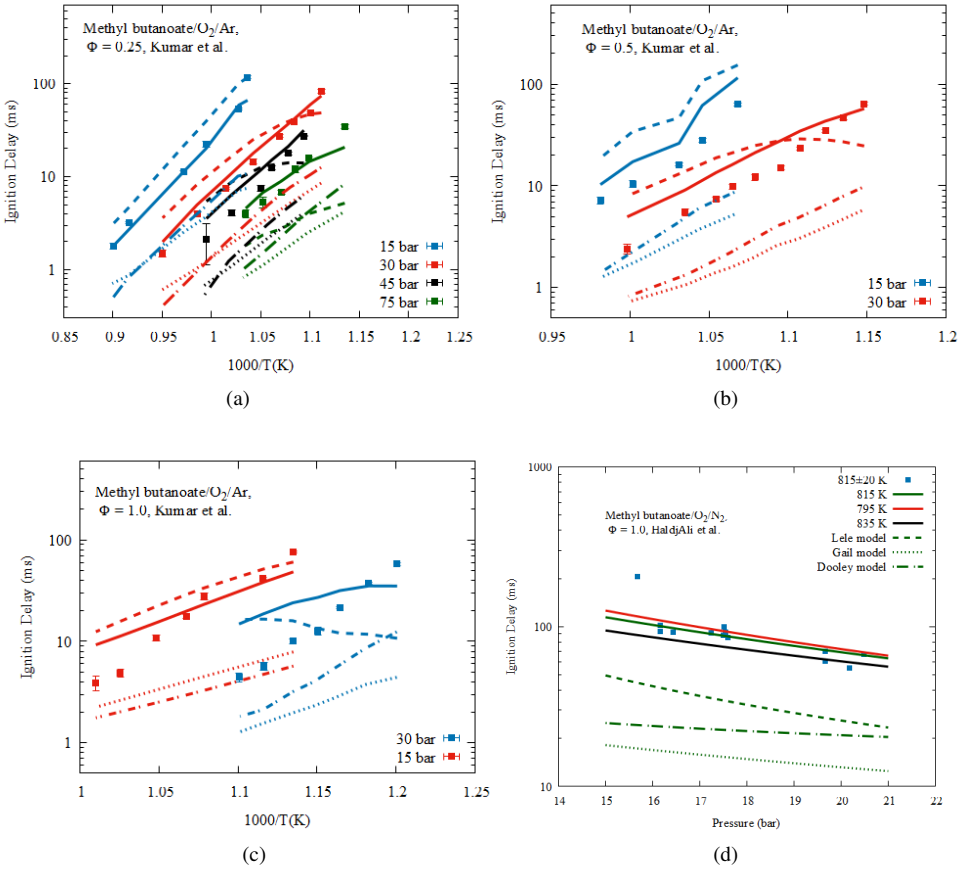


Fig. 26: Ignition delay times of MB/O₂/Ar mixtures [7] in a RCM at (a) $\phi = 0.25$, (b) $\phi = 0.5$, (c-d) $\phi = 1.5$ with varying pressures (15-75 bar). Plot (d) shows ignition delay times of MB/air mixtures at stoichiometric condition [21]. Simulation results are shown using present model (solid lines), Lele model (--- lines) [9], Gail model (.... lines) [12], and Dooley model (-.-. lines) [1].

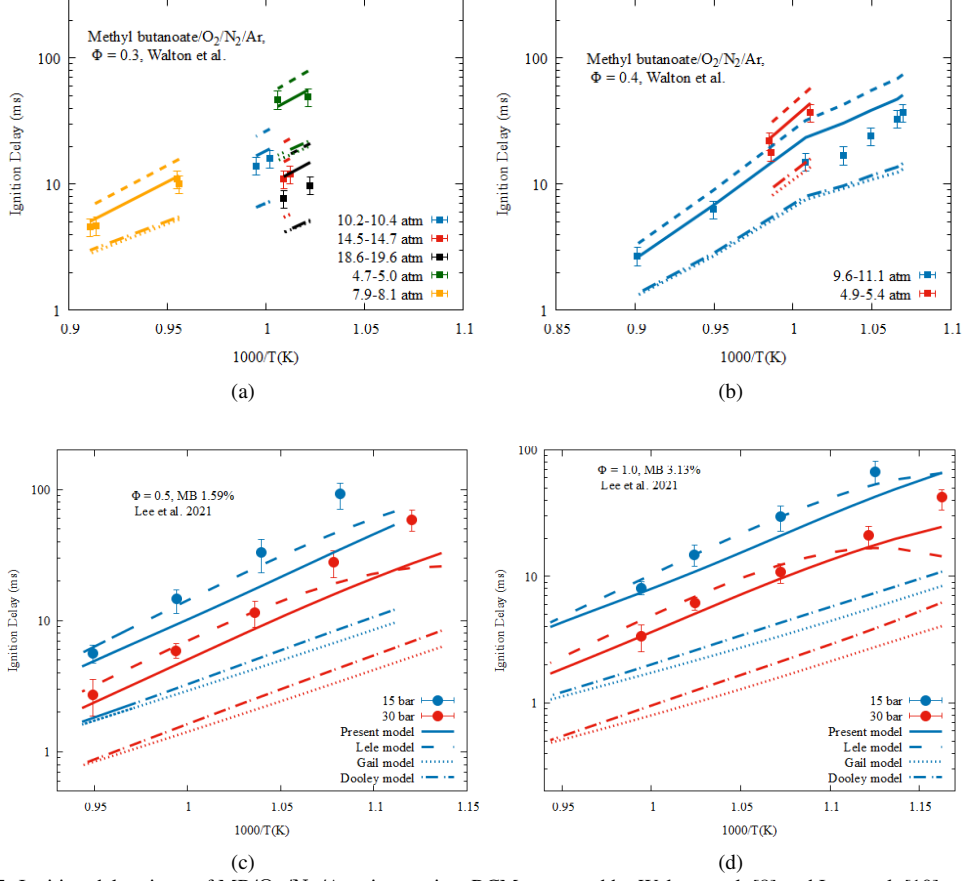


Fig. 27: Ignition delay times of MB/O₂/N₂/Ar mixtures in a RCM measured by Walton et al. [8] and Lee et al. [10] at equivalence ratios of (a) $\phi = 0.3$, (b) $\phi = 0.4$, (c) $\phi = 0.5$, and (d) $\phi = 1.0$. Symbols corresponds to experimental data points and lines show adiabatic simulation results using the present model (solid lines), Lele model (--- lines) [9], Gail model (.... lines) [12] and Dooley model (-.-. lines) [1].

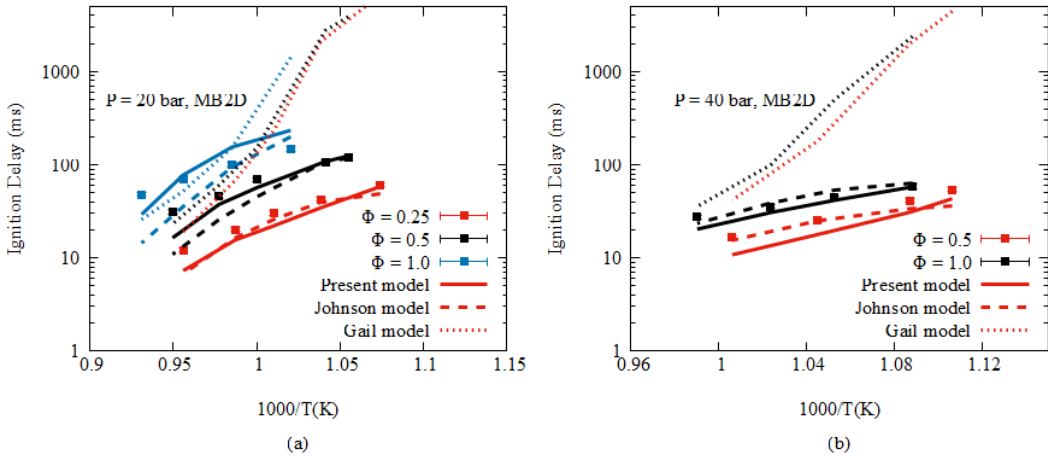


Fig. 28: Ignition delay times of MB2D/O₂/Ar/N₂ mixtures in a RCM at pressures of (a) $P = 20$ bar and (b) $P = 40$ bar for different equivalence ratios (0.25, 0.5, 1.0). Symbols correspond to experiment from Vallabhuni et al. [17] and line show simulation results using the present model (solid lines), Johnson model (--- lines) [15], and Gail model (.... lines) [12].

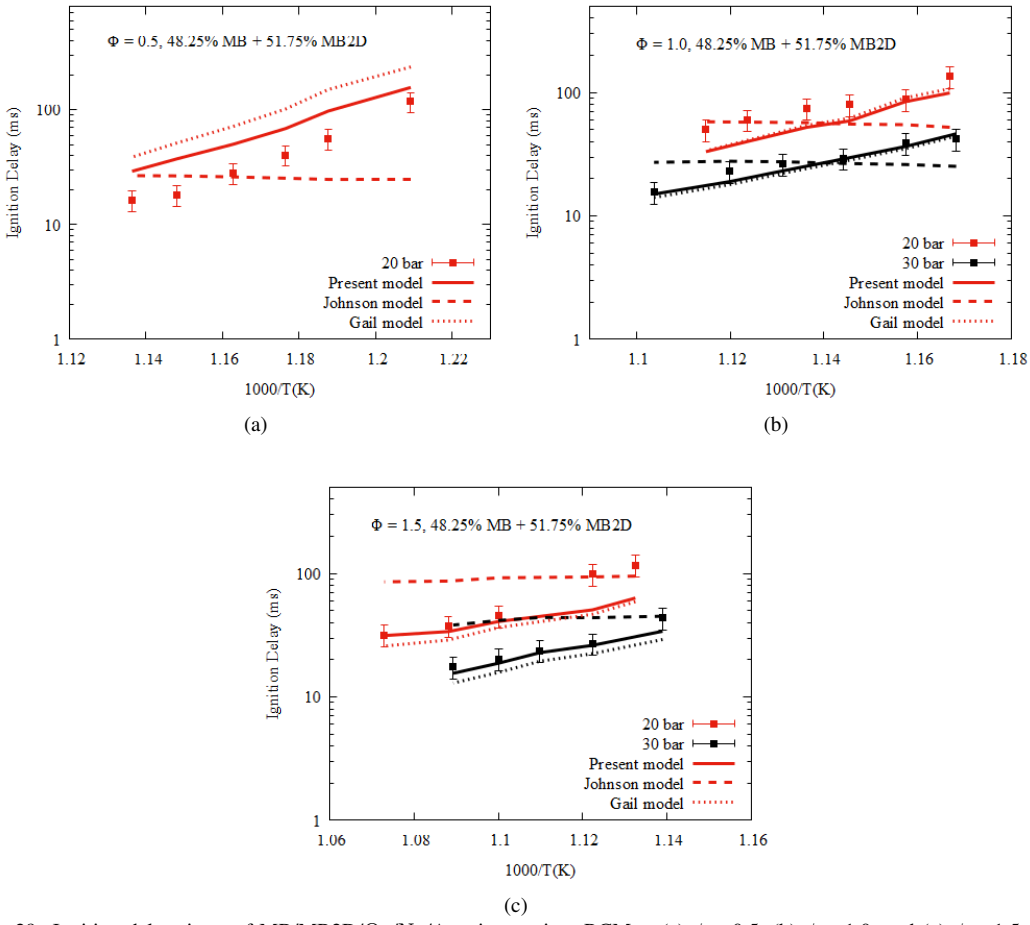


Fig. 29: Ignition delay times of MB/MB2D/O₂/N₂/Ar mixtures in a RCM at (a) $\phi = 0.5$, (b) $\phi = 1.0$, and (c) $\phi = 1.5$, for pressures of 20 and 30 bar. Symbols correspond to experimental data points and lines show simulation results using the present model (solid lines), Johnson model (- - - lines) [15], and Gail model (... lines) [12].

6. Path flux analysis

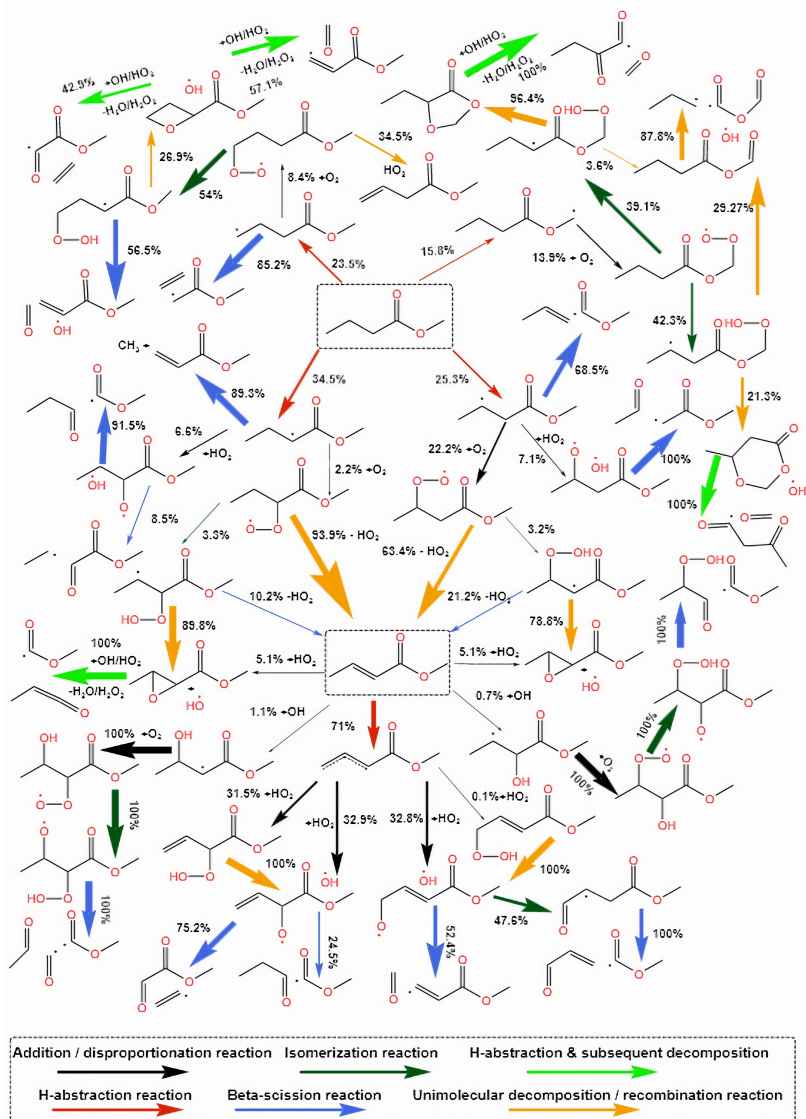


Fig. 30: Path flux analysis for oxidation of MB/O₂/N₂/Ar mixtures at $\phi = 1$ and P = 20 bar in isochor homogeneous reactor using present mechanism. Composition of mixture is given by 1.8% MB, 11.7% O₂, 43.25% N₂, and 43.25% Ar.

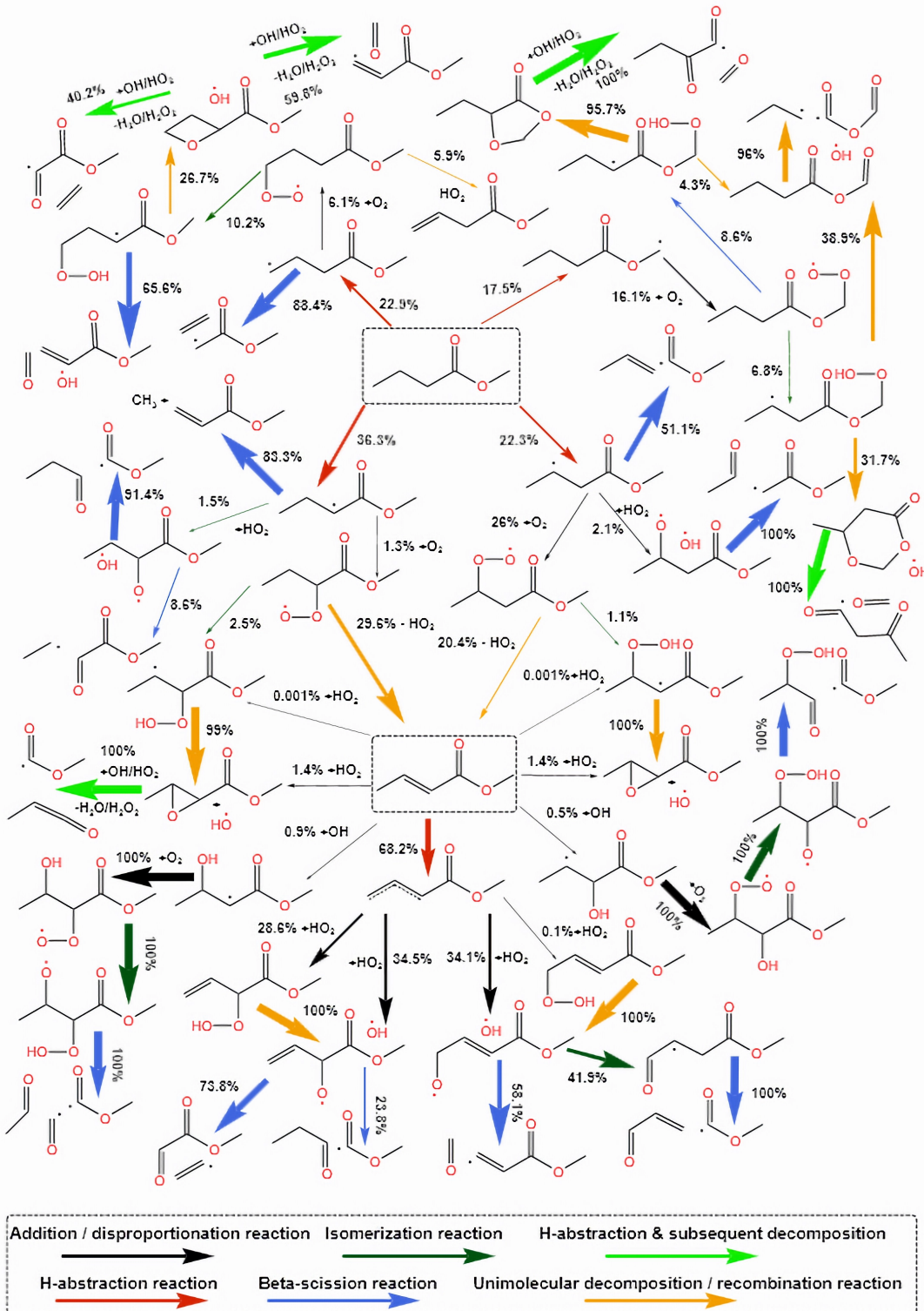


Fig. 31: Path flux analysis for oxidation of MB2D/O₂/N₂/Ar mixtures at $\phi = 1$ and P = 20 bar in isochor homogeneous reactor using present mechanism. Composition of mixture is given by 1.8% MB2D, 10.8% O₂, 43.7% N₂, and 43.7% Ar.

7. Effect of cross reactions on prediction of experimental data for blend of MB and MB2D

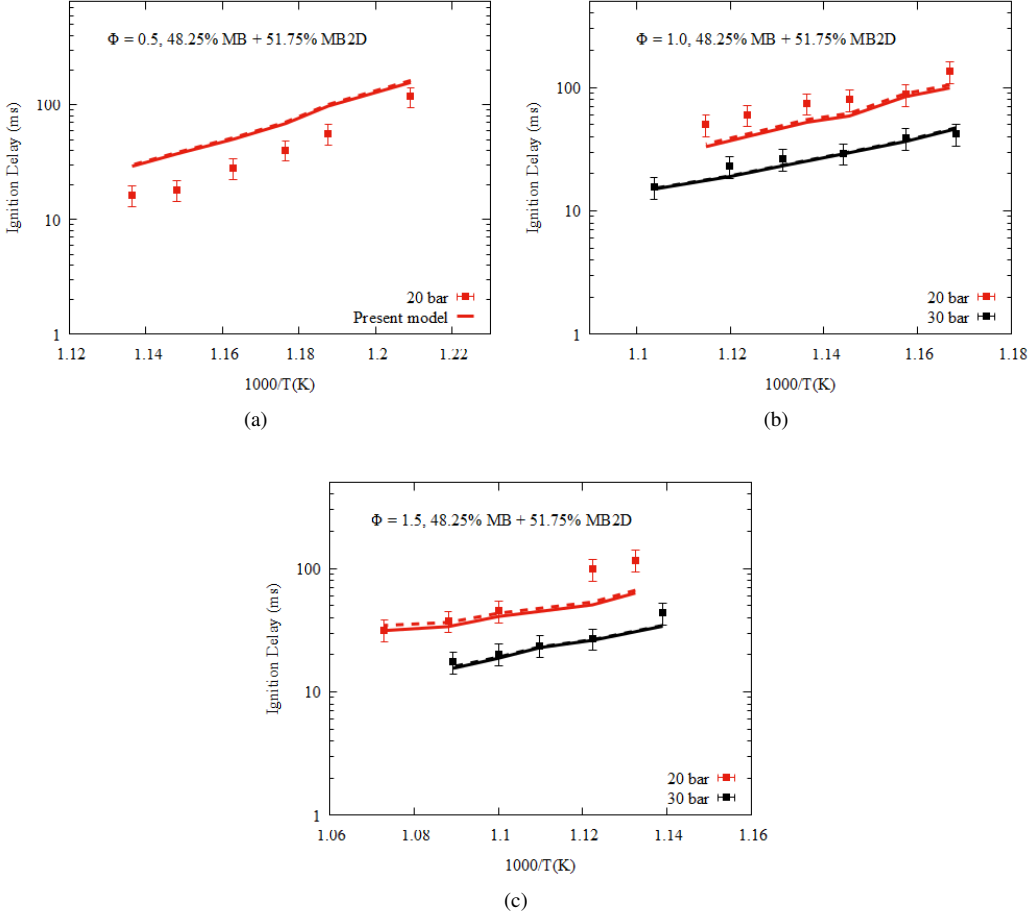


Fig. 32: Ignition delay times of MB/MB2D/O₂/N₂/Ar mixtures in a RCM at (a) $\phi = 0.5$, (b) $\phi = 1.0$, and (c) $\phi = 1.5$, for pressures of 20 and 30 bar. Symbols corresponds to experimental data points and comparison of simulation results using the present model (solid lines) and model without cross reactions (dashed lines).

8. List of newly added reactions

Reactions	Source
MB-C5H10O2=MP1J+CH3 MB-C5H10O2=NC3H7CO+CH3O MB-C5H10O2=MC3H6-OH+C2H4 MB-C5H10O2=AC3H6O2+C2H4 MB-C5H10O2=C5H10-3OH2 MB-C5H10O2=C3H7CHO+CH2O	[22]
MB3MOOH2J=>CH3CHOOHCCHCO+OCH2O2H MB3MOOH4J=>C2H3OOH+CH2CO+OCH2O2H MBM4OOH2J=>OH+CH2O+C2H3CO+OCH2O2H MB3DMOOH=>C3H5-A+CO2+CH2O+OH MB3D2OOH=>OH+C2H3CHO+CH3OCO MB3MOOH2J=>CH3CHOOHCCHCO+OCH2O2H MB3MOOH4J=>C2H3OOH+CH2CO+OCH2O2H MBM4OOH2J=>OH+CH2O+C2H3CO+OCH2O2H MB3DMOOH=>C3H5-A+CO2+CH2O+OH MB3D2OOH=>OH+C2H3CHO+CH3OCO	[23]
MB2D4J=C4H4O13+CH3O	[24]
MB2D+H=C3H5-S+CH3OCCHO MB2D+H=CH3O+SC3H5CHO MB2D+H=SC3H5CO+CH3+OH	[25]
MB2DO+OH=>CH3CHCO+CH3OCO+H2O MB3DO+OH=>CH2CO+ME2J+H2O MB4DO+OH=>C2H3CHO+CH3OCO+H2O MBMDO+OH=>C2H5CHCO+OCHO+H2O	[26]
MB2DO+HO2=>CH3CHCO+CH3OCO+H2O2 MB3DO+HO2=>CH2CO+ME2J+H2O2 MB4DO+HO2=>C2H3CHO+CH3OCO+H2O2 MBMDO+HO2=>C2H5CHCO+OCHO+H2O2	[27]
MB2OOH3J=MB2DO+OH MB2OOHMJ=MB2DO+OH MB2OOH4J=MB2DO+OH MB3OOH4J=MB3DO+OH MB4OOH2J=MB4DO+OH MBMOOH3J=MBMDO+OH	[28]

Table 2: List of newly added reaction in the chemistry of MB of present kinetic model.

Reactions	Source
$\text{MB2D4J} + \text{MB2J} = \text{MB2,3D} + \text{MB-C5H10O2}$ $\text{MB2D4J} + \text{MB3J} = \text{MB2,3D} + \text{MB-C5H10O2}$ $\text{MB2D4J} + \text{MB4J} = \text{MB2,3D} + \text{MB-C5H10O2}$ $\text{MB2D4J} + \text{MBMJ} = \text{MB2,3D} + \text{MB-C5H10O2}$ $\text{MB2D4J} + \text{MB2J} = 2\text{MB2D}$ $\text{MB2D4J} + \text{MB3J} = 2\text{MB2D}$ $\text{MB2D} + \text{MB2OO} = \text{MB2D4J} + \text{MB2OOH}$ $\text{MB2D} + \text{MB3OO} = \text{MB2D4J} + \text{MB3OOH}$ $\text{MB2D} + \text{MB4OO} = \text{MB2D4J} + \text{MB4OOH}$ $\text{MB2D} + \text{MBMOO} = \text{MB2D4J} + \text{MBMOOH}$	[29]
$\text{MB2D4J} + \text{MB-C5H10O2} = \text{MB2D} + \text{MB2J}$ $\text{MB2D4J} + \text{MB-C5H10O2} = \text{MB2D} + \text{MB3J}$ $\text{MB2D4J} + \text{MB-C5H10O2} = \text{MB2D} + \text{MB4J}$ $\text{MB2D4J} + \text{MB-C5H10O2} = \text{MB2D} + \text{MBMJ}$	[30]
$\text{MB2OO} + \text{MB2D4J} = \text{C5H7O3-B} + \text{MB2O}$ $\text{MB2OO} + \text{MB2D4J} = \text{C5H7O3-A} + \text{MB2O}$ $\text{MB3OO} + \text{MB2D4J} = \text{C5H7O3-B} + \text{MB3O}$ $\text{MB3OO} + \text{MB2D4J} = \text{C5H7O3-A} + \text{MB3O}$ $\text{MB4OO} + \text{MB2D4J} = \text{C5H7O3-B} + \text{MB4O}$ $\text{MB4OO} + \text{MB2D4J} = \text{C5H7O3-A} + \text{MB4O}$ $\text{MBMOO} + \text{MB2D4J} = \text{C5H7O3-B} + \text{MBMO}$ $\text{MBMOO} + \text{MB2D4J} = \text{C5H7O3-A} + \text{MBMO}$	[31]
$\text{MB2D} + \text{OH} = \text{MBOH-3J}$ $\text{MB2D} + \text{OH} = \text{MBOH-2J}$	[25]
$\text{MBOH-3J} + \text{O}_2 = \text{MBOH3OOJ}$ $\text{MBOH-2J} + \text{O}_2 = \text{MBOH2OOJ}$	[32]
$\text{MBOH3OOJ} = \text{MBOJ3OOH}$ $\text{MBOJ3OOH} = \text{CH3OCO} + \text{C3KET12}$ $\text{MBOH2OOJ} = \text{MBOJ2OOH}$ $\text{MBOJ2OOH} = \text{CH3CHO} + \text{HCO} + \text{CH3OCO} + \text{OH}$	[33]
$\text{MB2D4J} + \text{HO}_2 = \text{C5H7O3-B} + \text{OH}$ $\text{MB2D4J} + \text{HO}_2 = \text{MB1D3OOH}$ $\text{MB2D4J} + \text{HO}_2 = \text{C5H7O3-A} + \text{OH}$ $\text{MB2D4J} + \text{HO}_2 = \text{MB3D1OOH}$ $\text{MB1D3OOH} = \text{C5H7O3-B} + \text{OH}$ $\text{MB3D1OOH} = \text{C5H7O3-A} + \text{OH}$ $\text{C5H7O3-B} = \text{C2H3} + \text{C3H4O}_3$ $\text{C5H7O3-B} = \text{C2H3CHO} + \text{CH3OCO}$ $\text{C5H7O3-B} = \text{MB3J2O}$ $\text{C5H7O3-A} = \text{MB2J4O}$ $\text{MB3J2O} = \text{CH3CHCO} + \text{CH3OCO}$ $\text{MB2J4O} = \text{C2H3CHO} + \text{CH3OCO}$	[34]
$\text{C5H7O3-A} = \text{MP2D3J} + \text{CH2O}$	[35]
$\text{C3H4O}_3 = \text{HCO} + \text{CH3OCO}$	[36]

Table 3: List of newly added reaction in the chemistry of MB2D of present kinetic model.

References

- [1] S. Dooley, H. J. Curran, J. M. Simmie, Autoignition measurements and a validated kinetic model for the biodiesel surrogate, methyl butanoate, *Combust. Flame* 153 (1-2) (2008) 2–32.
- [2] M. H. Hakka, H. Bennadji, J. Biet, M. Yahyaoui, B. Sirjean, V. Warth, L. Coniglio, O. Herbinet, P.-A. Glaude, F. Billaud, et al., Oxidation of methyl and ethyl butanoates, *International Journal of Chemical Kinetics* 42 (4) (2010) 226–252.
- [3] A. A. Konnov, J. Chen, M. L. Lavadera, Measurements of the laminar burning velocities of small alkyl esters using the heat flux method: A comparative study, *Combust. Flame* 255 (2023) 112922.
- [4] Y. L. Wang, Q. Feng, F. N. Egolfopoulos, T. T. Tsotsis, Studies of c4 and c10 methyl ester flames, *Combust. Flame* 158 (8) (2011) 1507–1519.
- [5] W. Li, J. Zhang, S. Eckart, J. Xia, H. Krause, Y. Li, On the laminar flame propagation of c5h10o2 esters up to 10 atm: A comparative experimental and kinetic modeling study, *Proc. Combust. Inst.* 39 (2) (2023) 1851–1860.
- [6] B. Yang, C. K. Westbrook, T. A. Cool, N. Hansen, K. Kohse-Höinghaus, Fuel-specific influences on the composition of reaction intermediates in premixed flames of three c5h10o2 ester isomers, *Phys Chem Chem Phys* 13 (15) (2011) 6901–6913.
- [7] K. Kumar, C.-J. Sung, Autoignition of methyl butanoate under engine relevant conditions, *Combust. Flame* 171 (2016) 1–14.
- [8] S. Walton, M. Wooldridge, C. Westbrook, An experimental investigation of structural effects on the auto-ignition properties of two c5 esters, *Proc. Combust. Inst.* 32 (1) (2009) 255–262.
- [9] A. D. Lele, S. K. Vallabhuni, K. Moshammer, R. X. Fernandes, A. Krishnasamy, K. Narayanaswamy, Experimental and chemical kinetic modeling investigation of methyl butanoate as a component of biodiesel surrogate, *Combust. Flame* 197 (2018) 49–64.
- [10] S. Lee, S. Song, Hydrogen effects on ignition delay time of methyl butanoate in a rapid compression machine, *International Journal of Energy Research* 45 (4) (2021) 5602–5618.
- [11] A. J. Marchese, M. Angioletti, F. L. Dryer, Flow reactor studies of surrogate biodiesel fuels, in: *Proceedings of the 30th International Symposium on Combustion*, 2004, pp. 25–30.
- [12] S. Gaïl, S. Sarathy, M. Thomson, P. Diévert, P. Dagaut, Experimental and chemical kinetic modeling study of small methyl esters oxidation: Methyl (e)-2-butoenoate and methyl butanoate, *Combust. Flame* 155 (4) (2008) 635–650.
- [13] H. Bennadji, J. Biet, L. Coniglio-Jaubert, F. Billaud, P.-A. Glaude, F. Battin-Leclerc, Experimental autoignition of c4-c6 saturated and unsaturated methyl and ethyl esters, *arXiv preprint arXiv:0904.3539* (2009).
- [14] C. Li, M. Ye, B. Liu, Y. Shang, H. Ning, J. Shi, S.-N. Luo, Shock tube experiments and kinetic modeling of ignition of unsaturated c5 methyl esters, *Energy* 284 (2023) 128613.
- [15] P. N. Johnson, M. L. Lavadera, A. A. Konnov, K. Narayanaswamy, Oxidation kinetics of methyl crotonate: A comprehensive modeling and experimental study, *Combust. Flame* 229 (2021) 111409.
- [16] B. Yang, C. K. Westbrook, T. A. Cool, N. Hansen, K. Kohse-Höinghaus, Photoionization mass spectrometry and modeling study of premixed flames of three unsaturated c5h8o2 esters, *Proc. Combust. Inst.* 34 (1) (2013) 443–451.
- [17] S. Vallabhuni, P. Johnson, B. Shu, K. Narayanaswamy, R. Fernandes, Experimental and kinetic modeling studies on the auto-ignition of methyl crotonate at high pressures and intermediate temperatures, *Proc. Combust. Inst.* 38 (1) (2021) 223–231.
- [18] S. Davis, C. K. Law, Determination of and fuel structure effects on laminar flame speeds of c1 to c8 hydrocarbons, *Combustion Science and Technology* 140 (1-6) (1998) 427–449.
- [19] C. Olm, I. G. Zsély, R. Pálvölgyi, T. Varga, T. Nagy, H. J. Curran, T. Turányi, Comparison of the performance of several recent hydrogen combustion mechanisms, *Combustion and Flame* 161 (9) (2014) 2219–2234.
- [20] K. Kumar, C.-J. Sung, B. W. Weber, J. A. Bunnell, Autoignition of methyl propanoate and its comparisons with methyl ethanoate and methyl butanoate, *Combustion and Flame* 188 (2018) 116–128.
- [21] K. HadjAli, M. Crochet, G. Vanhove, M. Ribaucour, R. Minetti, A study of the low temperature autoignition of methyl esters, *Proc. Combust. Inst.* 32 (1) (2009) 239–246.
- [22] M. Akbar Ali, A. Violi, Reaction pathways for the thermal decomposition of methyl butanoate, *The J. Org. Chem.* 78 (12) (2013) 5898–5908.
- [23] S. M. Sarathy, C. K. Westbrook, M. Mehl, W. J. Pitz, C. Togbe, P. Dagaut, H. Wang, M. A. Oehlschlaeger, U. Niemann, K. Seshadri, et al., Comprehensive chemical kinetic modeling of the oxidation of 2-methylalkanes from c7 to c20, *Combust. Flame* 158 (12) (2011) 2338–2357.
- [24] Y. Sun, C.-W. Zhou, K. P. Somers, H. J. Curran, An ab initio/transition state theory study of the reactions of C5H9 species of relevance to 1, 3-pentadiene, part ii: Pressure dependent rate constants and implications for combustion modeling, *J. Phys. Chem. A* 124 (2020) 4605–4631.
- [25] L. Zhang, Q. Chen, P. Zhang, A theoretical kinetics study of the reactions of methylbutanoate with hydrogen and hydroxyl radicals, *Proc. Combust. Inst.* 35 (1) (2015) 481–489.
- [26] J. Mendes, C.-W. Zhou, H. J. Curran, Theoretical study of the rate constants for the hydrogen atom abstraction reactions of esters with• oh radicals, *The Journal of Physical Chemistry A* 118 (27) (2014) 4889–4899.
- [27] Q. Meng, L. Zhang, Q. Chen, Y. Chi, P. Zhang, Influence of torsional anharmonicity on the reactions of methyl butanoate with hydroperoxy radical, *The Journal of Physical Chemistry A* 124 (42) (2020) 8643–8652.
- [28] H. Tao, K. C. Lin, Pathways, kinetics and thermochemistry of methyl-ester peroxy radical decomposition in the low-temperature oxidation of methyl butanoate: A computational study of a biodiesel fuel surrogate, *Combust. Flame* 161 (9) (2014) 2270–2287.
- [29] D. Edelson, D. Allara, A computational analysis of the alkane pyrolysis mechanism: Sensitivity analysis of individual reaction steps, *International Journal of Chemical Kinetics* 12 (9) (1980) 605–621.
- [30] P. DAGAUT, M. CATHONNET, J.-C. BOETTNER, Propyne oxidation: A kinetic modeling study, *Combustion Science and Technology* 71 (1-3) (1990) 111–128.

- [31] N. Lokachari, S. Panigrahy, G. Kukkadapu, G. Kim, S. S. Vasu, W. J. Pitz, H. J. Curran, The influence of iso-butene kinetics on the reactivity of di-isobutylene and iso-octane, Combustion and Flame 222 (2020) 186–195.
- [32] A. Miyoshi, Molecular size dependent falloff rate constants for the recombination reactions of alkyl radicals with O_2 and implications for simplified kinetics of alkylperoxy radicals, International Journal of Chemical Kinetics 44 (1) (2012) 59–74.
- [33] Y. Li, Q. Zhao, Y. Zhang, Z. Huang, S. M. Sarathy, A systematic theoretical kinetics analysis for the waddington mechanism in the low-temperature oxidation of butene and butanol isomers, J. Phys. Chem. A 124 (27) (2020) 5646–5656.
- [34] C. F. Goldsmith, S. J. Klippenstein, W. H. Green, Theoretical rate coefficients for allyl+ HO_2 and allyloxy decomposition, Proc. Combust. Inst. 33 (1) (2011) 273–282.
- [35] G. Yin, C. F. Goldsmith, X. Chen, E. Hu, Z. Huang, Rate coefficients for 1, 2-dimethyl-allyl+ HO_2/O_2 and the implications for 2-methyl-2-butene combustion, Combustion and Flame 230 (2021) 111433.
- [36] W. Sun, B. Yang, N. Hansen, C. K. Westbrook, F. Zhang, G. Wang, K. Moshammer, C. K. Law, An experimental and kinetic modeling study on dimethyl carbonate (dmc) pyrolysis and combustion, Combustion and Flame 164 (2016) 224–238.